Harmonics Mitigation of a Solar PV-Fuel Cell Based Microgrid System using a Shunt Active Power Filter

Sarita Samal[1], **Prasanta Kumar Barik**[2†], and **Prakash Kumar Hota**[3], Non-members

ABSTRACT

The increased penetration of distributed energy resources is inspiring the entire design of conventional electrical power systems. A Microgrid (MG) includes distributed generation, loads, energy storage, and a control system capable of operating in grid-connected mode and/or island mode. The power quality (PQ) issue is one of the main technical challenges in an MG power system. To improve PQ, it is necessary to analyze the harmonic distortion of the system. Moreover, harmonic distortion in MG networks has significantly reduced PQ, affecting the stability of the system. The shunt active power filter (SAPF) has been extensively used to diminish the current harmonics and verified as being the best solution. Hence, in this paper, the impact of PQ issues in an adopted standalone MG system (comprising solar and fuel cell based renewable energy sources) is investigated in the presence of SAPF. The SAPF is realized using a conventional synchronous reference frame (SRF) technique for current generation with a pulse-width modulation voltage source inverter technique to generate pulses for the inverter along with a PI controller to regulate the DC-link capacitor voltage. The proposed model is developed in MATLAB/SIMULINK and the results validate the superiority of the proposed technique over others in terms of harmonic elimination.

Keywords: Fuel Cell, Harmonics, Microgrid, Shunt Active Power Filter

1. INTRODUCTION

The Microgrid (MG) represents the amalgamation of numerous energy sources, with a battery system whereby different electronic converters are connected either in grid or island mode [1]. In both modes, a power quality (PQ) problem exists due to the use of nonlinear loads. Harmonic generation is the main PQ issue due to the connection of a nonlinear load [2]. The word harmonic is extensively used to illustrate the distortion of voltage or current waveforms [3, 4]. Harmonic-related problems occur due to nonlinear loads distrusting the supply voltage [5]. Active power filters (APF) are advanced to reimburse the reactive power and harmonics at the same time [6]. Active filters may be connected in series, shunt, or a mixture of both along with hybrid arrangements [7–10].

The use of shunt active power filters (SAPF) for current harmonic compensation typically in domestic, commercial, and industrial applications is explained in Montero *et al.* [11]. Jain *et al.* [12] presented their experimental investigations and design/simulation on a shunt active power filter for harmonics and reactive power compensation. Moreover, most of the control strategies in previous literature focus only on a grid-connected system whereas in the MG system, the design of the controller is often neglected. To ensure stable operation and improve the system performance of MG in island mode, the SAPF is used at the point of common coupling (PCC), compensating the harmonics of the load current. The MG system considered in this paper represents the integration of solar photovoltaics and a fuel cell with the shunt APF [13]. The solar photovoltaic system is connected to a boost converter, the output of which depends upon the pulses generated from the maximum power point tracking system. From the many methods of MPPT, the perturb and observe (P&O) technique is selected by the researcher due to its simplicity and cost-effectiveness. Femia *et al.* [14] developed a scheme to optimize the P&O maximum power point tracking method. However, a fuel cell is environmentally friendly, noise-free, and highly efficient in comparison to other sources [15, 16]. It can be interfaced with AC and DC distribution systems using different electronic devices, as described by Kalirasu *et al.* [17]. Samal and Hota [18], and Nergaard *et al.* [19] designed a 48 V fuel cell with an inverter application and ultra-capacitor for

Manuscript received on October 1, 2019 ; revised on October 13, 2020 ; accepted on January 7, 2021. This paper was recommended by Associate Editor Kriangkrai Sooksood.

[1]The author is with the Department of Electrical Engineering, Kalinga Institute of Industrial Technology, India.

[2]The author is with the Department of Mechanical and Electrical Engineering, College of Agricultural Engineering and Technology, Orissa University of Agriculture and Technology, India.

[3]The author is with the Department of Electrical Engineering, Veer Surendra Sai University of Technology, India.

[†]Corresponding author: prasantbarik05@gmail.com

Digital Object Identifier 10.37936/ecti-eec.2021192.222556

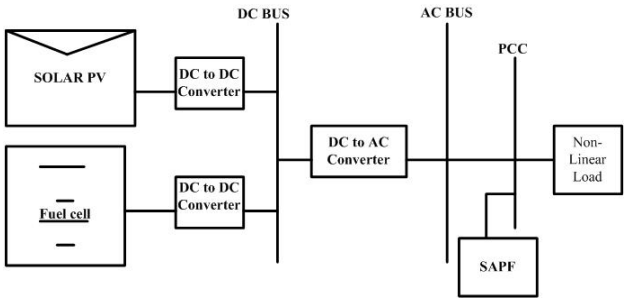

Fig. 1: *Basic block diagram of a microgrid.*

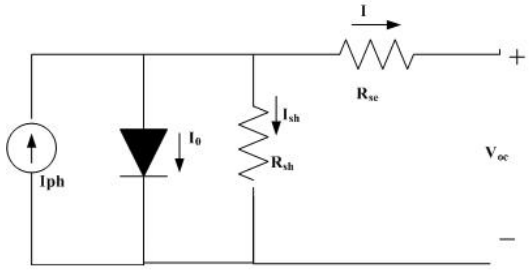

Fig. 2: *Solar cell single diode model.*

energy storage purposes. Bucci *et al.* [20] described the various types of fuel cell technology using MATLAB modeling and the implementation of a proton exchange membrane (PEM) fuel cell. Despite numerous studies being conducted on power PQ analysis using the SAPF for grid-connected systems, the standalone mode has mostly been ignored.

Hence, this paper focuses on the PQ analysis of an MG (solar PV and fuel cell) system operated in standalone mode. According to the previous literature, the realization of SAPFs mostly depends on three significant factors, namely the control technique employed for (a) referencing current generation, (b) regulation of DC-link capacitor voltage, and (c) generation of switching pulses for the inverter [21]. In most of the reported works, the current generation employs the conventional synchronous reference frame (SRF) technique [22]. A study of the literature reveals that PI controllers have been widely used for DC-link voltage control of the SAPFs to enhance the PQ level of an MG system operated under the grid-connected mode. Whereas hardly any work on the application of the SRF technique based on the SAPF has been carried out on the standalone mode MG system. Therefore, this has motivated the authors of this study to further investigate the PQ issues involved in the adopted islanded MG system in the presence of SAPF using the SRF approach to reference current generation with a PI controller for DC-link voltage control.

The main contributions of the current work are as follows.

(a) An MG system comprising solar PV and fuel cell based RES, modeled using the standalone mode of operation.
(b) Use of the SRF to design a PI controller and hysteresis current controller (HCC) with the pulse width modulation (PWM) technique based on the SAPF for the adopted MG system.
(c) A comparative study using the proposed technique with and without the SAPF.

The remainder of this paper is organized as follows. Section 2, the design of the proposed DG system is described, while Section 3 presents the SAPF model with its different control schemes. The simulation results are presented in Section 4, showing the effectiveness of the proposed algorithm in comparison to conventional algorithms. Finally, Section 5 provides a brief conclusion, summarizing the significant contributions of the work.

2. PROPOSED SYSTEM

A basic block diagram of the MG system with the SAPF, demonstrating the configuration of a solar PV-fuel cell, coupled to a common DC bus is shown in Fig. 1. From the DC bus, the power is converted into AC with the help of a power inverter, while the SAPF is placed in between the grid and nonlinear load.

2.1 Modeling of Solar PV

The principle of solar PV is that when light energy falls on a solar cell it is converted into electrical energy. The single diode model equivalent circuit of a solar PV system is shown in Fig. 2 with the photocurrent represented by I_{ph}, while I and I_{sh} are the currents through the series resistance R_{se} and shunt resistance R_{sh}, respectively [14]. All other parameters required for the design of the solar module are shown in Eqs. (1)–(5).

$$I = I_{ph} - I_0 - I_{sh} \tag{1}$$

$$I_{ph} = [I_{sc} + K_i\,(T - T_r)] \times \frac{G}{1000} \tag{2}$$

$$I_{rs} = \frac{I_{sc}}{\exp\left(\dfrac{qV_{OC}}{N_S kAT}\right) - 1} \tag{3}$$

$$I_0 = I_{rs}\left(\frac{T}{T_r}\right)^3 \exp\left(\frac{qV_{OC}}{Ak}\left[\frac{1}{T_r} - \frac{1}{T}\right]\right) \tag{4}$$

$$I_{PV} = N_P I_{ph} - N_P I_0\left[\exp\left(\frac{qV_{PV} + I_{PV}R_{se}}{N_S kAT}\right) - 1\right] \tag{5}$$

where I_{sc} is the short circuit current, K_i is the short circuit current of cell at 25 °C and 1000 W/m^2, T is the oprating temperature of the p-n junction, T_r is the rated temperature, G is the operataing solar radiation, I_{rs} is the reverse saturation current, q is the electron charge $= 1.6 \times 10^{-19}$ C, k is the Boltzmann's

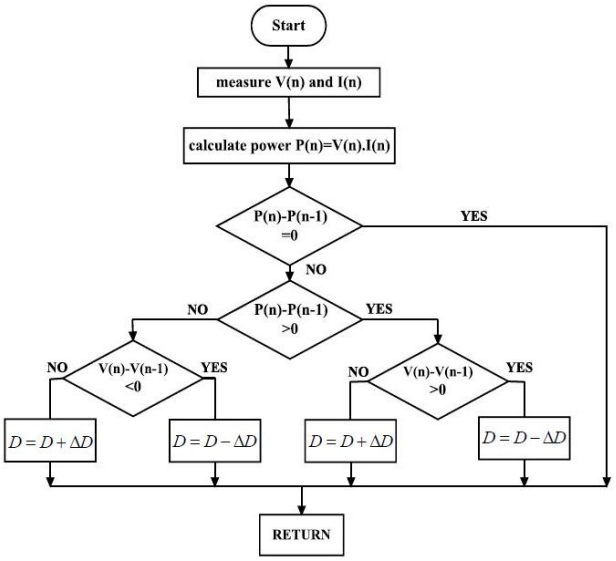

Fig. 3: *Flowchart of the P&O MPPT algorithm.*

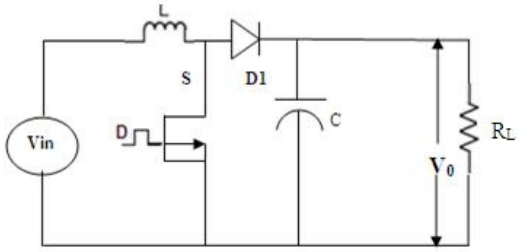

Fig. 4: *Boost converter.*

constant $= 1.3805 \times 10^{-23}$ J/K, A is the ideality factor of the diode, N_S is the number of cells connected in series, N_P is the number of cells connected in parallel, V_{OC} is the open-circuit voltage, V_{PV} is the diode voltage, and I_{PV} is the photo current of the diode.

A. Perturb and Observe MPPT Algorithm

To increase the efficiency of the solar panel, use of the maximum power point (MPP) technique is essential. Although many methods are available in the literature for obtaining maximum power from the PV cell, the perturb and observe (P&O) approach is the simplest and easiest to implement. Therefore, the P&O MPPT algorithm is selected for use in this study due to its simplicity and cost-effectiveness. Using this algorithm, firstly the PV panel terminal voltage $V(n)$ and current $I(n)$ are calculated and the related value of the power measured, denoted by $P(n)$. The detailed flow chart in Fig. 3 describes the algorithm for designing the MPP system using the P&O technique where $V(n)$ is the PV panel terminal voltage, $V(n-1)$ is the voltage due to perturbation, $I(n)$ is the PV panel current, $P(n)$ is the PV panel power, $P(n-1)$ is the power due to perturbation, D is the duty cycle of the boost converter, and ΔD is the change in duty cycle.

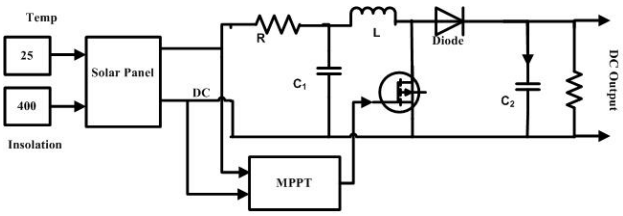

Fig. 5: *Simulation of Solar PV with the MPPT and boost converter.*

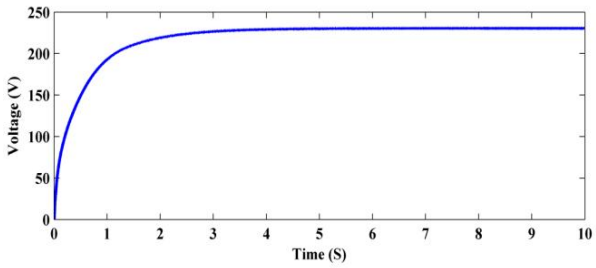

Fig. 6: *Output voltage.*

B. Step-up Converter

A step-up converter is a device which increases the solar voltage to the desired output as required by the load. Fig. 4 shows the configuration of the boost converter, consisting of an inductor L, DC input voltage V_{in}, switch S, capacitor C, diode D_1, and load resistance R_L. By turning ON switch S, the boost inductor stores the energy fed from the input voltage source. By turning OFF switch S, the input voltage and the stored inductor voltage appear across the load, thereby increasing the load voltage [15, 16]. If the switch operates with duty cycle D, then the DC voltage output is given by Eq. (6).

$$\frac{V_o}{V_{in}} = \frac{1}{1-D} \tag{6}$$

C. Simulation of the PV System

In general, the efficiency of a PV unit is extremely low; therefore, it is essential to operate the PV unit at its peak point so that the highest level of power can be provided to the load in any condition. A step-up converter placed subsequent to the PV unit, consumes peak power with the help of the P&O MPPT method to match the impedance of the circuit with the PV unit impedance. Impedance matching is possible by varying the duty cycle of the boost converter. The simulation of solar PV with the P&O MPPT and step-up converter is shown in Fig. 5, while the boost converter output voltage is shown in Fig. 6. Table 1 shows the parameters required for the design of a boost converter.

Table 1: *Boost converter parameters.*

Parameters	Ratings
Supply voltage	80 V
Inductance at source side (L)	0.01 H
Resistance at source side (R)	1 Ω
Capacitance at source side (C_1)	0.002 F
Capacitance at load (C_2)	0.002 F
Load resistance (R_L)	24 Ω
Output voltage	230 V

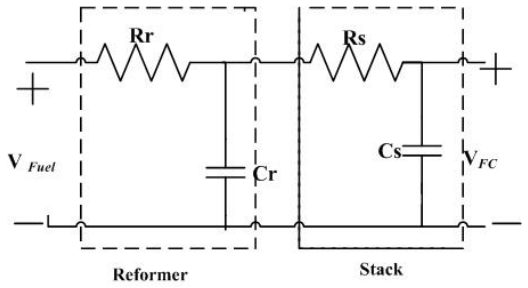

Fig. 7: *Fuel cell equivalent circuit.*

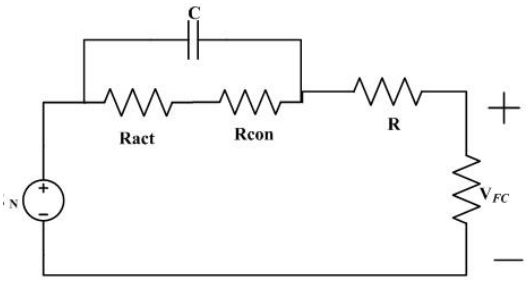

Fig. 8: *Simplified model of a single PEM cell.*

2.2 PEM Fuel Cell Model

The fuel cell is a device which produces electricity from the chemical reaction between hydrogen and oxygen [17]. The reformer is presented by a first order equation with the corresponding transfer function shown in Eq. (7). The stack is also represented by a first order time delay equation with the transfer function shown in Eq. (8).

$$\frac{V_{cr}}{V_{in}} = \frac{\dfrac{1}{C_r s}}{R_r + \dfrac{1}{C_r s}} = \frac{1}{1 + R_r C_r s} = \frac{1}{1 + \tau_r s} \tag{7}$$

$$\frac{V_{cs}}{V_{cr}} = \frac{\dfrac{1}{C_s s}}{R_s + \frac{1}{C_s s}} = \frac{1}{1 + R_s C_s s} = \frac{1}{1 + \tau_s s} \tag{8}$$

The electrochemical equivalent model of a fuel cell is shown in Fig. 7. The mathematical model for the design of a PEM fuel cell using different sets of equations is shown in the form of Eqs. (9)–(16), while the simplified PEM model is shown in Fig. 8.

Table 2: *Different fuel cell parameters.*

Parameters	Ratings
V_{OC}	65 V
Number of cells	65
Stack efficiency	55%
Airflow rate	300 IPM
Fuel cell resistance	0.70833 Ω
Load resistance (R_{load})	5 Ω
One cell voltage	1.128 V
H_2	99.56%
O_2	59.3%

$$E_N = 1.229 - 0.00085\,(T - 298.15) + 4.31 \times 10^{-5} \times T\left[\ln\left(P_{H2}\right) + \frac{1}{2}\ln\left(P_{O2}\right)\right] \tag{9}$$

$$V_{FC} = E_N - V_{act} - V_{Ohmic} - V_{con} \tag{10}$$

$$V_{act} = -\left[\xi_1 + \xi_2 T + \xi_3 T \ln\left(CO_2\right)\right] \tag{11}$$

$$CO_2 = \frac{P_{O2}}{5.08 \times 10^6 \times \exp\left(-\dfrac{498}{T}\right)} \tag{12}$$

$$V_{Ohmic} = i_{FC}\left(R_M + R_C\right) \tag{13}$$

$$R_M = \frac{\rho_M \lambda}{A} \tag{14}$$

$$V_{con} = \ln\left(1 - \frac{J}{J_{\max}}\right) \times (-B) \tag{15}$$

$$V_s = kV_{FC} \tag{16}$$

where E_N is the open-circuit thermodynamic potential of the cell. Each cell model parametric coefficients are represented by ξ_1, ξ_2, ξ_3, ξ_4, and Ψ. V_{Ohmic} is the ohmic voltage drop, R_M is the proton conduction equivalent membrane resistance, R_C is the electron conduction equivalent contact resistance, V_{con} is the concentration over potential, k is the number of cells connected in series, A is the membrane area in cm^2, R is the contact resistance in ohm, C is the capacitance in farad, $J_{\max}$ is the maximum current density in $\mathrm{A/cm}^2$, P_{H2} is the pressure of hydrogen (atm), P_{O2} is the pressure of oxygen (atm), and T is the temperature in Kelvin.

A. Simulation of a Fuel Cell with Boost Converter

A simple fuel cell typically produces an output voltage ranging from 0.5–0.9 V. Since this low voltage is insufficient for real-time applications, a stack of fuel cells is arranged in series with a step-up converter connected so that the required voltage can be achieved. A simulation diagram of a fuel cell with a step-up converter is shown in Fig. 9. The output voltage of the step-up converter is shown in Fig. 10, while Table 2 shows the different parameters required for fuel cell simulation.

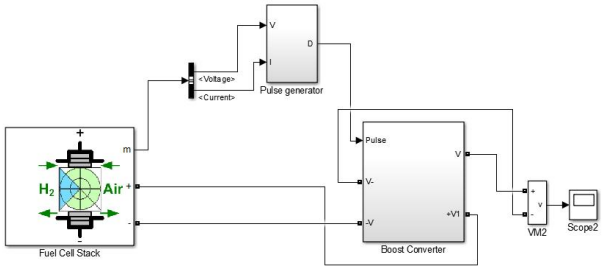

Fig. 9: *Fuel cell with boost converter.*

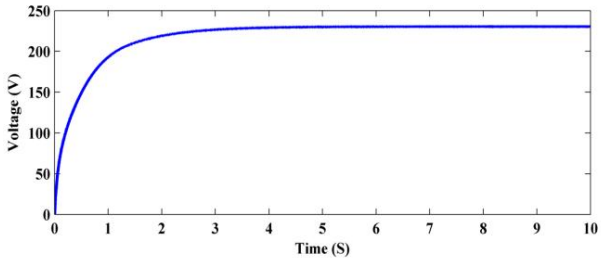

Fig. 10: *Output voltage of boost converter.*

3. DESIGN OF A SHUNT ACTIVE POWER FILTER

The SAPF is normally connected in parallel to the system, indicating the harmonic content. Fig. 11 shows the basic structure of a shunt active filter. To remove the harmonics, an identical amount of harmonic compensating current is injected in the reverse phase w.r.t harmonic current. The shunt active power filter injects the compensating current into the PCC such that the load current becomes harmonic free.

This compensating current cancels out the current harmonics, rendering the load current sinusoidal. Therefore, the SAPF is used to eradicate current harmonics and reimburse the reactive power on the source side, thereby making the load current harmonic free. Eqs. (17) and (18) show instantaneous current and the source voltage, respectively.

$$I_s(t) = I_L(t) - I_c(t) \tag{17}$$

$$V_s(t) = V_m \sin \omega t \tag{18}$$

The Fourier series method is used to express the nonlinear load current as shown in Eq. (19).

$$I_s(t) = I_1 \sin(\omega t + \Phi_1) + \sum_{n=2}^{\varepsilon} I_n \sin(n\omega t + \Phi_n) \tag{19}$$

The compensation current of the active filter can be expressed by:

$$I_c(t) = I_L(t) - I_s(t) \tag{20}$$

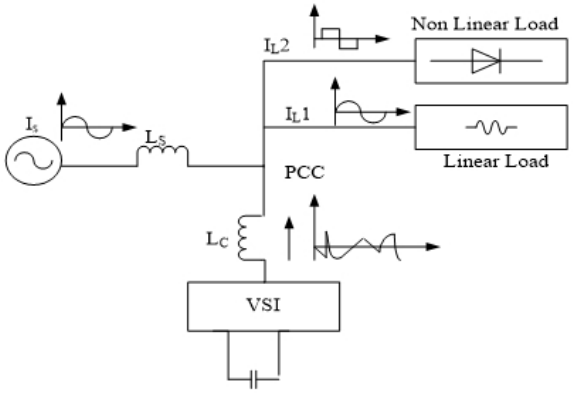

Fig. 11: *Basic structure of the shunt active filter.*

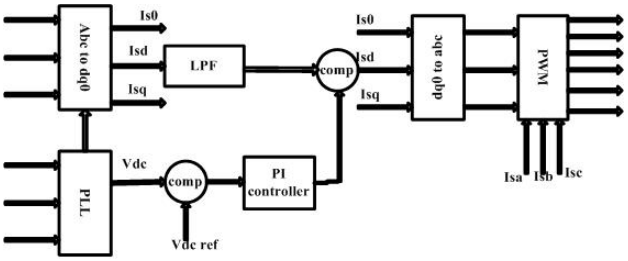

Fig. 12: *SRF control method.*

Hence, for the exact compensation of reactive power and harmonics, it is essential to determine $I_s(t)$. The instantaneous value of source, load, and compensation current can be expressed by $I_s(t)$, $I_L(t)$, and $I_c(t)$ where, $V_s(t)$ and V_m correspond to the instantaneous value and peak value of source voltage.

3.1 Control Method for SAPF

The SRF controller scheme works in steady-state and dynamic conditions to completely control the reactive power in distribution and reduce the harmonics in load current. There are many control methods available for SAPF, here the design basic SRF method is used for easy implementation. The normal arrangement of the SRF system contains a phase-locked loop (PLL) unit for vector orientation as shown in Fig. 12. The control method consists of the transfer of source current from *abc* to *d-q*. The three-phase load currents I_{La}, I_{Lb}, and I_{Lc} are converted to I_d-I_q using the transformation technique given in Eq. (21).

$$\begin{bmatrix} i_q \\ i_d \\ i_0 \end{bmatrix} = \frac{2}{3} \begin{bmatrix} \cos\theta & \cos(\theta - 120) & \cos(\theta + 120) \\ \sin\theta & \sin(\theta - 120) & \sin(\theta + 120) \\ \frac{1}{2} & \frac{1}{2} & \frac{1}{2} \end{bmatrix} \begin{bmatrix} i_{La} \\ i_{Lb} \\ i_{Lc} \end{bmatrix} \tag{21}$$

With a nonlinear load, the source current includes both oscillating and dc components. To maintain

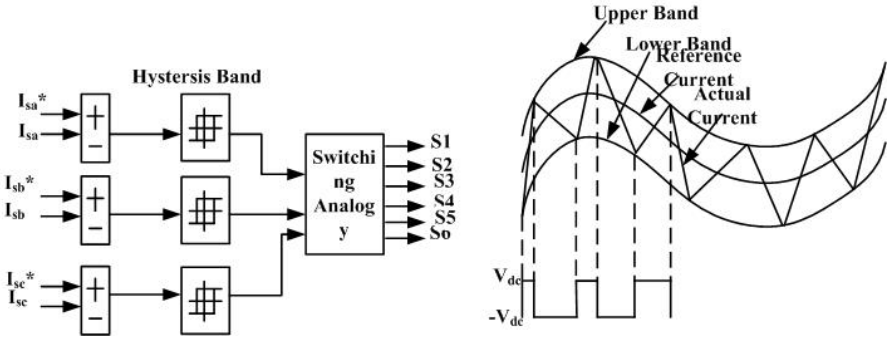

Fig. 13: *Hysteresis current controller.*

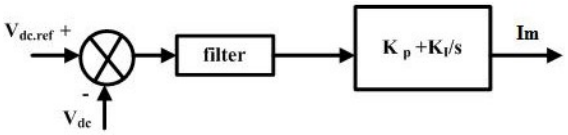

Fig. 14: *PI controller model.*

voltage across the link capacitor, an active filter absorbs some of the active power from the system. The shunt active filter eliminates the harmonics component present in the source current, rendering the current wave source sinusoidal.

3.2 Hysteresis Band Current Controller

Fig. 13 shows a block diagram of the hysteresis current regulator and the switching of pulse generation to the voltage source inverter. In the current regulator, the error signal is generated by comparing the reference current $I_{sa}{}^*$ and actual current I_{sa} [20].

3.3 DC-Link Voltage Control

The active and reactive power flow to the system is provided by the DC-link capacitor when required. The PI controller is a common control loop feedback method widely used in industrial control systems and other applications. The PI controller algorithm has two separate parameters: proportional (P) and integral (I). The proportional value determines the reaction to current error, while the integral value determines the reaction based on the sum of recent errors. The equation for PI controller is given in Eq. (22),

$$I_m = e_n K_p + e_n K_i dt \tag{22}$$

where K_p and K_i represent the proportional and integral gains, respectively. I_m represents the output of the controller. The voltage error value e_n is fed into the PI controller. The basic model of the PI controller is shown in Fig. 14 .

In order to preserve the DC-link voltage at the reference value, the DC-link capacitor requires a certain amount of real power, proportionate to the difference between the actual and reference voltages. The power requisite for the DC-link capacitor can be expressed as in Eq. (23).

$$P_{dc} = e_n K_p + e_n K_i dt \tag{23}$$

If the values of K_p and K_i are large, the DC-bus voltage regulation is leading and the steady-state DC-bus voltage error low. On the other hand, if K_p and K_i are small, the real power imbalance has little effect on the transient performance. Therefore, the proper election of K_p and K_i are basically important to ensure control performance and maintain the requisite capacitor power. In the first approach, K_p and K_i values are chosen as 0.8 and 23, respectively based on trial and error.

4. RESULTS AND DISCUSSION

The Simulink model for the MG PV-fuel cell system is shown in Fig. 15. The performance of the proposed model is analyzed under the following operating conditions (referred to as scenarios).

- Scenario 1: MG connected to a nonlinear load without SAPF.
- Scenario 2: MG connected to a nonlinear load with an SRF-PI-based SAPF.

4.1 Performance Analysis under Scenario 1

In this case, the system performance is analyzed by firstly connecting a nonlinear load to the MG system without SAPF. It is perceived that the load current waveform is non-sinusoidal and the THD is very high at almost 16.66%. Fig. 16 shows the source current waveform, while Fig. 17 presents the THD content using fast Fourier transform (FFT) analysis.

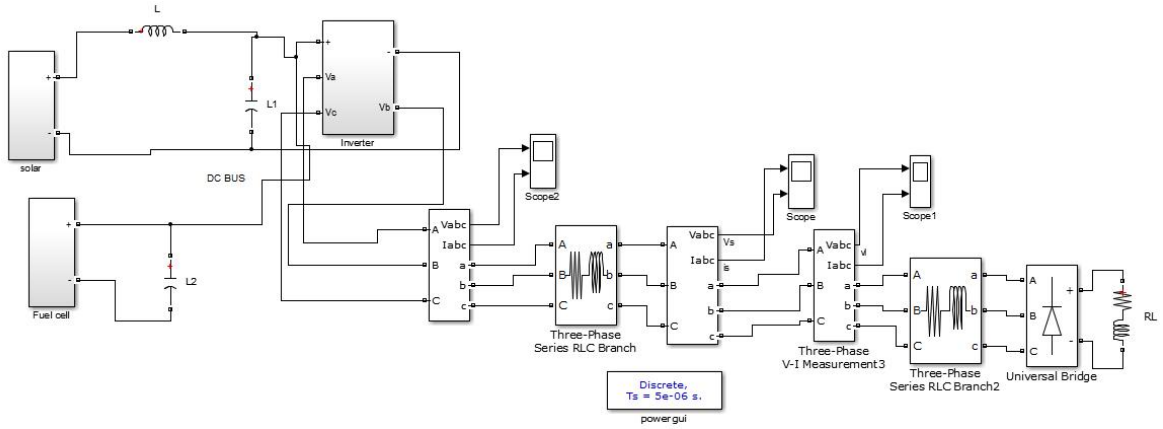

Fig. 15: *Microgrid with a nonlinear load without the SAPF.*

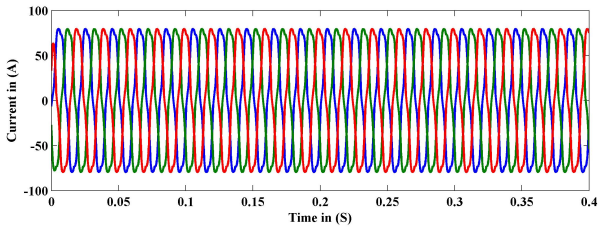

Fig. 16: *Load current without the SAPF.*

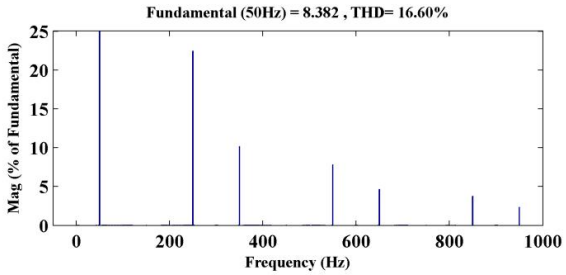

Fig. 17: *Harmonic analysis without the SAPF.*

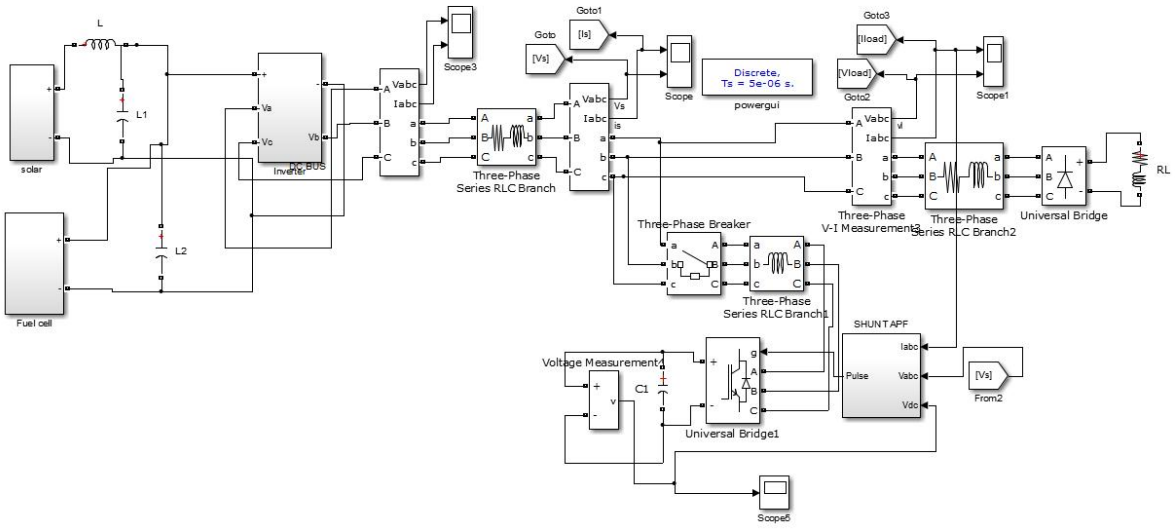

Fig. 18: *Simulink Model of Microgrid with nonlinear load and SAPF.*

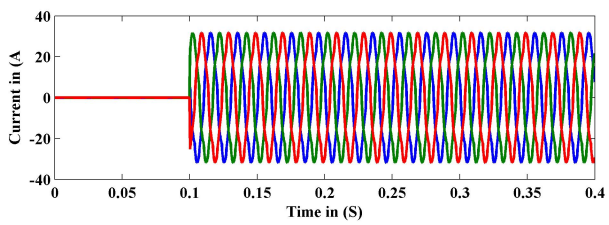

Fig. 19: *Current injected by SRF based SAPF.*

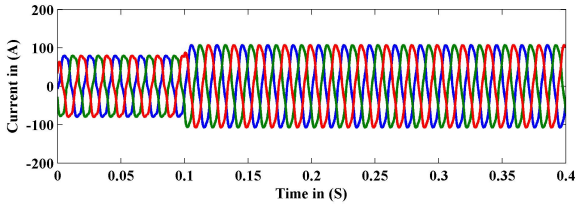

Fig. 20: *Load current with SRF based SAPF.*

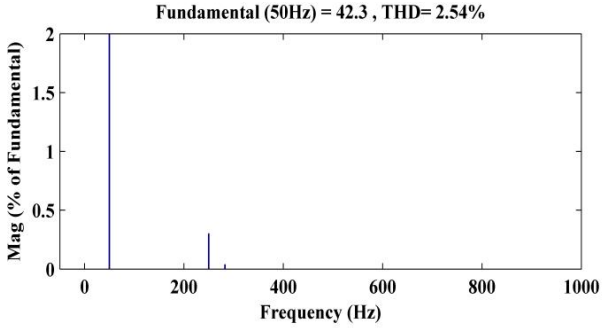

Fig. 21: *Harmonics analysis SRF based SAPF.*

4.2 Performance Analysis under Scenario 2

In this scenario, the SAPF is connected to the MG and the system performance analyzed. Fig. 18 shows the MG with SAPF. The SAPF is turned on at between 0.1 and 0.4 s. Fig. 19 shows the compensating current injected by the SAPF using the SRF method on the PCC. The load current harmonics are reduced to 2.54% as shown in the FFT analysis in Fig. 20, with the load current being almost sinusoidal and harmonic free, as shown in Fig. 21.

5. CONCLUSION

The performance of the SAPF under different conditions was studied and compared with the SRF method. The harmonics in load current were observed to reduce to below 5% in all cases. The suggested method delivered superior output compared to the existing method in terms of voltage regulation and harmonic mitigation. The implementation of MG with SAPF has the advantage of being able to compensate for all the power quality problems in any load conditions. The simulation results show that the load current harmonics are compensated when a nonlinear load is connected. The analysis revealed that the MG with the SAPF can compensate for all the PQ issues on the distribution side.

REFERENCES

[1] C. Benachaiba, A. M. A. Haidar, M. Habab, and O. Abdelkhalek, "Smart Control of UPCQ within Microgrid Energy System," *Energy Procedia*, vol. 6, pp. 503–512, 2011.

[2] R. Ahmadi and M.Ferdowsi, "Improving the Performance of a Line Regulating Converter in a Converter-Dominated DC Microgrid System," *IEEE Transactions on Smart Grid*, vol. 5, no. 5, pp. 2553–2563, 2014.

[3] B. Singh, K. Al-Haddad, and A. Chandra, "A review of active filters for power quality improvement," *IEEE Transactions on Industrial Electronics*, vol. 46, no. 5, pp. 960–971, 1999.

[4] N. Zaveri and A. Chudasama "Control strategies for harmonic mitigation and power factor correction using shunt active filter under various source voltage conditions," *Electrical Power and Energy Systems*, vol. 42, no. 1, pp. 661–671, Nov. 2012.

[5] R. Arnold, "Solutions to the power quality problem," *Power Engineering Journal*, vol. 15, no. 2, pp. 65–73, April 2001.

[6] P. Karuppanan and K. K. Mahapatra, "PI, PID and Fuzzy Logic Controlled Cascaded Voltage Source Inverter based Active Filter for Power Line Conditioners," *WSEAS Transaction on Power Systems*, vol. 6, no. 4, pp. 100–109, Oct. 2011.

[7] S. Samal and P. K. Hota, "Power Quality Improvement by Solar Photo-voltaic/Wind Energy Integrated System Using Unified Power Quality Conditioner," *International Journal of Power Electronics and Drive Systems*, vol. 8, no. 3, pp. 1416–1424, 2017.

[8] S. Samal and P. K. Hota, "Power Quality Improvement by Solar Photo-voltaic/Fuel Cell Integrated System Using Unified Power Quality Conditioner," *International Journal of Renewable Energy Research*, vol. 7, no. 4, pp. 2075–2084, 2017.

[9] S. Samal and P. K. Hota, "Design and analysis of solar PV-fuel cell and wind energy based microgrid system for power quality improvement," *Cogent Engineering*, no. 4, 2017, Art. no. 1402453.

[10] M. A. Hannan and A. Mohamed, "PSCAD/EMTDC Simulation of Unified Series-Shunt Compensator for Power Quality Improvement," *IEEE Transaction on Power Delivery*, vol. 20, no. 2, pp. 1650–1656, April 2005.

[11] W. M. Grady, M. J. Samotyj, and A. H. Noyola, "Survey of Active Power Line Conditioning Methodologies," IEEE Transaction on Power Delivery, vol. 5, no. 3, pp. 1536–1542, July 1990.

[12] M. I. M. Montero, E. R. Cadaval, and F. B. Gonzalez, "Comparison of control strategies for shunt active power filters in three-phase four-wire systems," *IEEE Transactions on Power Electronics*, vol. 22, no. 1, pp. 229–236, 2007.

[13] S. K. Jain, P. Agarwal, and H. O. Gupta, "Simulation and experimental investigations on a shunt active power filter for harmonics and reactive power compensation," *IETE Technical Review*, vol. 20, no. 6, pp. 481–492, 2003.

[14] N. Femia, G. Petrone, G. Spagnuolo, and M. Vitelli, "Optimization of perturb and observe maximum power point tracking method," *IEEE Transactions on Power Electronic*, vol. 20, no. 4, pp. 963–973, 2005.

[15] I. H. Altas and A. M. Sharaf, "A photovoltaic array simulation model for Matlab-Simulink GUI environment," in *2007 International Confer-*

ence on Clean Electrical Power (ICCEP), 2007, pp. 341–345.

[16] J. Viinamäki, J. Jokipii, T. Messo, T. Suntio, M. Sitbon, and A. Kuperman, "Comprehensive dynamic analysis of photovoltaic generator interfacing DC-DC boost power stage," *IET Renewable Power Generation*, vol. 9, no. 4, pp. 306–314, 2015.

[17] A. Kalirasu and S. S. Dash, "Simulation of closed loop controlled boost converter for solar installation," *Serbian Journal of Electrical Engineering*, vol. 7, pp. 121–130, 2010.

[18] S. Samal and P. K. Hota, "Wind Energy Fed UPQC System for Power Quality Improvement," *Bulletin of Electrical Engineering and Informatics*, vol. 7, no. 3, pp. 495–504, 2018.

[19] T. A. Nergaard, J. F. Ferrell, L. G. Leslie, and J.-S. Lai, "Design considerations for a 48 V fuel cell to split single phase inverter system with ultracapacitor energy storage," in *Proceedings of the 2002 IEEE 33rd Annual IEEE Power Electronics Specialists Conference (PES)*, 2002, pp. 2007–2012, vol. 4.

[20] G. Bucci, F. Ciancetta, E. Fiorucci, and F. Veglio, "An experimental approach to the modeling of PEM fuel cells in dynamic conditions," in *2007 IEEE Lausanne Power Tech*, 2007, pp. 1094–1099.

[21] P. Karuppanan and K. K. Mahapatra, "PI and fuzzy logic controllers for shunt active power filter—A report," *ISA Transactions*, vol. 51, no. 1, Jan. 2012, Art. no. 163169.

[22] R. Patel and A. K. Panda, "Real time implementation of PI and fuzzy logic controller based 3-phase 4-wire interleaved buck active power filter for mitigation of harmonics with i_d–i_q control strategy," *International Journal of Electrical Power & Energy Systems*, vol. 59, pp. 66–78, July 2014.

Sarita Samal received her B.Tech. (Hons) in Electrical Engineering from Berhampur University, India, her M.Tech. in Power System Engineering from Veer Surendra Sai University of Technology (VSST), Burla, India, and Ph.D. from VSSUT. Her current research interests include power quality improvement and application of power electronics with non-conventional energy sources.

Prasanta Kumar Barik received his B.Tech. in Electrical Engineering from Utkal University, India, and M.Tech. in Power Electronics and drives from Kalinga Institute of Industrial Technology, India. He is pursuing his Ph.D. at Indian Institute of Technology (Indian School of Mines) Dhanbad, India. His current research interests include power quality improvement and application of power electronics with non-conventional energy sources.

Prakash Kumar Hota received his B.E. (Distinction) in Electrical & Electronics Engineering from National Institute of Technology Tiruchirapalli, India, his M.Sc. (Engineering) in Industrial Power Control & Electric Drives from Sambalpur University, Odisha, India, and his Ph.D. from Jadavpur University, Kolkata, India. He has published over 121 articles in different journals & conferences. He guided 10 Ph.D. scholars and is presently guiding seven scholars in the area of power system operation and control, deregulation, power quality, and hybrid generation systems.